JOURNAL OF CATALYSIS 150, 94–104 (1994)

Alumina-Supported Manganese Oxide Catalysts

I. Characterization: Effect of Precursor and Loading

Freek Kapteijn,[1,*] A. Dick van Langeveld,* Jacob A. Moulijn,* Amedeo Andreïni,† Michael A. Vuurman,† Andrzej M. Turek,‡ Jih-Mirn Jehng,‡ and Israel E. Wachs‡

*Department of Chemical Engineering, Delft University of Technology, Julianalaan 136, 2628BL Delft, The Netherlands; †Department of Chemical Engineering, University of Amsterdam, Nieuwe Achtergracht 166, 1018WV Amsterdam, The Netherlands; and ‡Zettlemoyer Center for Surface Studies and Department of Chemical Engineering, Lehigh University, Bethlehem, Pennsylvania 18015

Received June 17, 1993; revised April 13, 1994

Alumina-supported manganese oxide catalysts were prepared by two different routes, from Mn acetate and from Mn nitrate, and characterized by temperature-programmed reduction (TPR), Raman spectroscopy, X-ray photoelectron spectroscopy (XPS), and infrared spectroscopy. The characterization studies clearly showed that the two different preparations result in significantly different supported manganese oxide phases. The nitrate precursor resulted primarily in manganese oxide [Mn(III) and Mn(IV)] microcrystals 2–4 nm in size deposited mainly at the outer region of the alumina particles, while the acetate precursor resulted mainly in a highly dispersed surface manganese oxide phase [Mn(III)], homogeneously distributed throughout the alumina particles. These different states of the manganese oxide are reflected in the reduction properties of the alumina-supported manganese oxide phases (peak positions, sharpness, and extent of reduction). The origin of these differences is related, on the one hand, to the presence of the nitrate, which leads to agglomeration and oxidation of the Mn, and on the other hand, to the ion-exchange mechanism of Mn with surface hydroxyl groups in the acetate preparation route.

INTRODUCTION

Manganese oxides have long been known as catalytic materials. In 1820 Döbereiner (1) had already recognized the catalytic activity of MnO_2 in the decomposition of potassium perchlorate in aqueous solutions. Subsequently, manganese oxide became well known for its activity in the decomposition of hydrogen peroxide (2–4). Among the other reactions catalyzed by pure or supported oxides of manganese are CO oxidation (4–6) [especially when promoted by copper oxide or cobalt oxide (7)]; oxygen isotopic exchange (6); nitrous oxide decomposition (8); ozone decomposition (9); oxidation of methanol (10), ethylene (11), ammonia (12–14), nitric oxide (15) and tarry compounds in self-cleaning oven walls (9); catalytic combustion of methane (16) and volatile organic compounds (VOC) (9); oxidative coupling of methane (17, 18); hydrogenation of ethylene (10); and selective catalytic reduction (SCR) of NO with NH_3 (13, 14, 19) and its sulfidation for regenerative high-temperature H_2S removal (20). In all these reactions, the manganese oxide undergoes oxidation–reduction cycles, which reflects the ease of changing the oxidation state of the manganese ion. Despite the application of Mn catalysts to so many important catalytic reactions, only a few studies have appeared on the characterization of supported manganese oxides. Alumina-supported catalysts were studied by X-ray diffraction (XRD) (8, 10, 21, 22), magnetic susceptibility (8, 23, 24), electron spin resonance (ESR) (24, 25), X-ray photoelectron spectroscopy (XPS) (4, 22), Raman spectroscopy and ion scattering spectroscopy (ISS) (22), transmission electron microscopy (TEM) (21), phosphorescence spectroscopy (24), IR (4, 26), and diffuse reflectance spectroscopy (4). Only a few other supports have been examined (14, 23, 24, 26).

Manganese nitrate has been used in the preparation of the supported system in nearly all studies, probably because of its high solubility and the ease of removal of the nitrate anion during calcination. The calcination temperature has been found to determine the final oxidation state of the supported manganese oxide. On an alumina support MnO_2 is formed mainly below 700 K and Mn_2O_3 is formed at 900 K (4, 22, 23). Reduction at high temperatures in H_2 (900 K) is proposed to result in the formation of surface $MnAl_2O_4$ at loadings below 4 wt% and in MnO at higher loadings (8).

The manganese oxide dispersion of the ex-nitrate catalysts turned out to be poor, since manganese oxide XRD patterns were already observed above 2 wt% Mn loadings (21, 22). Moreover, XPS and ISS indicated that above 8 wt% Mn, the dispersion decreased further due to particle size growth. Other preparation techniques have also been

[1] To whom correspondence should be addressed.

0021-9517/94 $6.00

applied, such as *in situ* precipitation of manganese hydroxide (4, 10) and use of ammonium permanganate (4), which are thought to result in higher dispersions. In a recent study we used manganese(II)acetate in the preparation of alumina-supported manganese oxide catalysts for low-temperature SCR (13, 14) and H_2S removal reactions (20). The ex-acetate manganese oxide catalysts were found to be superior to the ex-nitrate samples. This was ascribed to the higher dispersion of the supported manganese oxide phase since no crystalline manganese oxide XRD patterns could be observed up to 15 wt% Mn.

This interesting observation prompted a systematic study of the alumina-supported manganese oxide catalysts as a function of Mn loading and the precursor in the SCR reaction, to explain its high activity and selectivity behavior as a function of these parameters at temperatures between 320 and 470 K (13, 14). This first article deals with the characterization of alumina-supported manganese oxide catalysts by different techniques: temperature-programmed reduction (TPR), XPS, and IR and Raman spectroscopy. Following articles will focus on the interaction of NO and NH_3 with these catalysts studied by *in situ* infrared spectroscopy and on the selective catalytic reduction and ammonia oxidation over these catalysts under steady state and transient conditions, in the latter case employing labeled molecules.

EXPERIMENTAL

Catalysts

The catalysts were prepared by pore volume impregnation of dried (395 K) γ-Al_2O_3 (Ketjen 000-1.5E CK300, S_{BET} = 200 m^2/g, pore volume V_p = 0.5 cm^3/g, particle size d_P = 210–250 μm) with aqueous solutions of $Mn(NO_3)_2 \cdot 4H_2O$ (Merck) or $MnAc_2 \cdot 4H_2O$ (Aldrich), where Ac signifies acetate. The pH of the impregnation solutions was in the ranges 3–5 and 6.7–7.5, respectively, depending on the concentration. The catalysts were subsequently dried by slowly heating to 400 K and calcined in air at 770 K for 3 h. A series of catalysts were prepared with Mn loadings of 1, 2, 4.5, 6, and 8.4 wt%. Samples of 6 wt% were also calcined at 870 and 970 K to examine the influence of calcination temperature. Due to the limited solubility of the acetate precursor, the preparation procedure was adapted in such a way that for all loadings, the impregnation was carried out in two stages with drying inbetween. This was done with both precursors to maintain comparable preparation procedures. Fairly homogeneously colored batches (ranging from pale tan to dark brown) were obtained in this way from the acetate precursor, and somewhat less homogeneous ones from the nitrate precursor. XRD did not reveal crystalline manganese oxide phases for any of the samples.

Acetic acid vapor was noted during impregnation with the acetate solution and NO_2 escaped during drying of the samples impregnated with the nitrate solution. Characteristics of the catalysts studied are given in Table 1.

TABLE 1

Characteristics of the Alumina-Supported Manganese Oxide Catalysts

wt% Mn	Number of impregnations	Mn atoms/nm^2
1	2	0.55
2	2	1.1
4.5	2	2.5
6	3	3.5
8.4	3	5.0

For reference manganese oxide compounds commercial samples of MnO_2 and Mn_2O_3 were used (Merck); Mn_3O_4 was prepared by slow reduction of MnO_2 at 473 K in H_2. These samples exhibited high crystallinity and specific surface areas below 3 m^2/g. In addition, MnO_2 and Mn_2O_3 were also prepared from $MnCO_3$ (14, 27), resulting in surface areas of 82 and 51 m^2/g, respectively. $MnAl_2O_4$ was prepared by mixing stoichiometric amounts of manganese(II)nitrate and aluminum nitrate and slowly heating in air to 770 K to obtain a mixed oxide. This sample was subsequently reduced in H_2 by TPR (10 K/min) up to 1400 K (soak time 4 h) and XRD confirmed the formation of $MnAl_2O_4$ (JCPDS File 29-880).

Temperature-Programmed Reduction

TPR experiments were carried out in a conventional apparatus equipped with a Permapure tubular drier to remove water from the reduction process and a thermocouple detector (TCD) to measure the H_2 consumption. The total flow used (20 cm^3/min) corresponded to 14 μmol/s (66% H_2 in Ar), and a heating rate of 10 K/min was employed. Calibration of the TCD was performed by injection of known amounts of Ar in the H_2/Ar flow, thus simulating H_2 consumption. This is an easy, quick, and highly reproducible method. In all cases the same amount of manganese was used in the reactor (1.2 mg). As a reference, 120 mg alumina sample was examined (corresponding to the amount of the 1 wt% Mn catalyst). The experimental conditions were such that the Monti–Baiker parameter (28) amounted to about 4, which could easily be achieved due to the high sensitivity of the system and the high signal-to-noise ratio.

Infrared Spectroscopy

Fourier transform infrared (FTIR) spectra were recorded on a Bio-Rad FTS-7 spectrometer (resolution 2 cm^{-1}) in an *in situ* transmission cell under air at 770 K to obtain dehydration conditions. For monitoring the surface

hydroxyl stretching region (3000–4000 cm^{-1}), self-supporting wafers of 8 mg (~10 mg/cm^2) were used and 1000 scans were averaged.

Raman Spectroscopy

The Raman spectra were recorded under ambient conditions at room temperature with a Spectra-Physics Ar^+ laser (Model 171). Typically, about 100–120 mW of the 514.5-nm line of the argon ion laser was used because of the poor scattering properties of the dark samples. To minimize fluorescence the samples were first recalcined in air at 770 K for 16 h prior to the Raman analysis. About 10–20 mg of the sample was pressed into a thin pellet 1 mm thick with a KBr backing for support. The sample, mounted in the holder, was spun at 2000 rpm to avoid local heating effects. The Raman spectra were recorded on a Triplemate spectrometer (Spex, Model 1877) coupled to a multichannel analyzer (Princeton Applied Research, Model 1463) equipped with an intensified photodiode array detector (1024 pixels, cooled to −35°C, resolution 2 cm^{-1}).

X-Ray Photoelectron Spectroscopy

XPS analysis was performed on a Perkin–Elmer Phi 5400 ESCA system equipped with a hemispherical analyzer. Mg$K\alpha$ radiation was used for sample excitation. Samples were prepared by pressing the catalyst onto an In foil. The region between 600 and 730 eV contains information on the Mn $2p_{3/2}$ and $2p_{1/2}$ electron excitations and Auger valence band transitions. Weak contributions of In excitations were removed by computer subtraction. The recording times ranged between 20 and 700 min depending on the Mn loading.

The average C 1*s* binding energy found on the In was 285.1 eV and was used as an internal reference for the C 1*s* on the catalyst samples to correct for charge shifts. This was in agreement with the findings of Strohmeier and Hercules (22). Use of the Al 2*p* line [74.5 eV (22)] of the alumina support yielded similar results for the binding energies within ±0.1 eV.

XPS intensity ratios were determined from the total integrated areas of the Mn $2p_{3/2}$ and Al 2*p* photoelectron lines. The background was assumed to be linear over the peak width.

RESULTS

Temperature-Programmed Reduction

TPR patterns of the ex-acetate and ex-nitrate catalysts are presented in Figs. 1A and B, respectively, as a function of Mn loading. The alumina support, included in Fig. 1A, trace a, revealed a reduction around 1100 K. This is also present in the other samples, but not always visible due to the changing manganese oxide/alumina ratio and/or the sharpness of the reduction peaks (ex-nitrate samples). This reduction was excluded from the quantification of the oxidation state of the manganese.

All samples also showed a peak in the temperature region 350–400 K, a consequence of an artifact due to desorption of gases (N_2, Ar, or CO_2), which are not removed after the reaction in the way that the produced water is, thus giving rise to an apparent H_2 consumption.

The ex-acetate samples (Fig. 1A) exhibit a manganese oxide reduction pattern over a broad temperature range (400–900 K) as a convolution of broad and overlapping peaks. All these samples have a reduction around 840 K which does not shift and remains constant per amount of alumina. The major reduction peak is situated around 650 K at 1 wt% Mn (trace b) and shifts monotonically to 580 K with increasing loading. A third reduction peak can be found around 500 K as a minor feature for 1 and 2 wt% Mn (traces a and b) and becomes pronounced for higher Mn loadings (traces d–f) while shifting to lower temperatures.

A two-step reduction profile is observed for all the ex-nitrate samples (Fig. 1B) and the ratio of the first (580–600 K) to the second (660–685 K) reduction peak slightly increases with increasing manganese loading from 1.5 to 2. A minor shift in the TPR peaks to lower temperatures is also observed with increasing loading, but is not as pronounced as for the ex-acetate samples. The 1 wt% Mn sample (trace a) also exhibits minor features at 500 and 840 K, similar to the ex-acetate samples. Calcination in air at higher temperatures (870 and 970 K) does not change the pattern significantly for the 6 wt% Mn ex-acetate sample (trace e). Only the low-temperature side of the broad reduction region decreases a little. In the case of the ex-nitrate catalyst, the high-temperature calcination results in essentially the disappearance of the strong peak at 580–610 K and the appearance of a weak third reduction visible as a shoulder around 720 K. Consequently, the reduction peak at 660–685 K becomes the dominant peak.

The total H_2 consumption is converted into an average O/Mn atomic ratio on the catalyst, assuming that the reduction ends with MnO, and is presented in Fig. 2A. This ratio slightly increases from 1.45 to 1.50 for the ex-acetate samples as a function of Mn loading. For the ex-nitrate samples the ratio is much higher, ranging from 1.55 to 1.80. The effect of heat treatment on the 6 wt% Mn samples is given in Fig. 2B. The O/Mn ratio of the ex-nitrate sample decreased most at 870 K to 1.47, whereas the ex-acetate sample exhibited the strongest decrease, to a ratio 1.33, at 970 K.

Infrared Spectroscopy

FTIR spectra of the hydroxyl stretching region for the alumina support and the alumina-supported Mn oxide

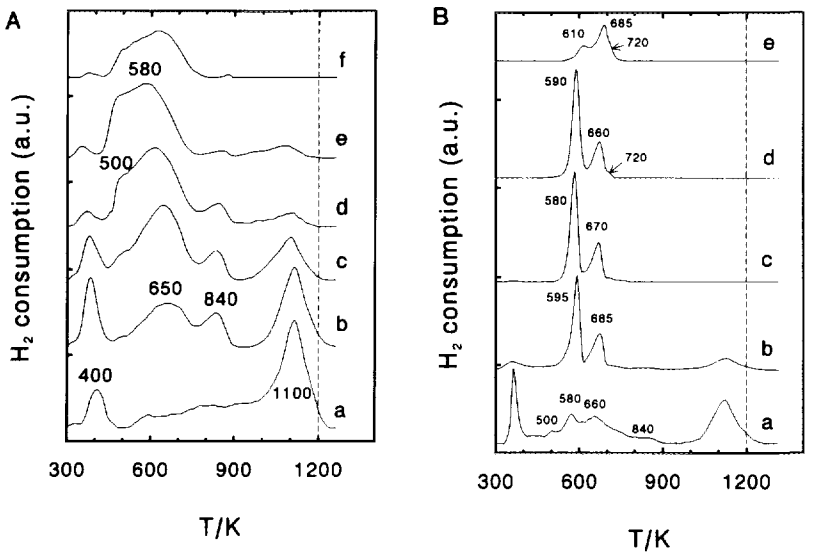

FIG. 1. Temperature-programmed reduction patterns of manganese oxide/alumina catalysts for various loadings. Heating rate: 10 K/min. (A) Ex-acetate samples: (a) γ-Al_2O_3; Mn loading—(b) 1 wt%, (c) 2 wt%, (d) 4.5 wt%, (e) 6 wt%, (f) 6 wt% calcined at 970 K. (B) Ex-nitrate samples: Mn loading—(a) 1 wt%, (b) 2 wt%, (c) 4.5 wt%, (d) 6 wt%, (e) 6 wt% calcined at 970 K.

samples are presented in Fig. 3. Three major absorption bands of alumina can be distinguished: 3775 cm^{-1} (basic –OH groups), 3730 cm^{-1} (neutral –OH groups), and 3680 cm^{-1} (acidic –OH groups) (29, 30). With increasing Mn loading the 3680 cm^{-1} band decreases continuously for the ex-acetate samples, and for the 6 wt% Mn sample (trace c) the 3775 cm^{-1} band also diminishes. For the 2 wt% Mn ex-nitrate sample (trace d) the 3775 cm^{-1} band has nearly vanished, whereas the 3680 cm^{-1} band has diminished slightly relative to the alumina. The 6 wt% Mn sample was too dark to yield spectra of sufficient quality and is not shown.

Raman Spectroscopy

Not much research has been performed on manganese oxide catalytic materials and therefore the Raman spectra of the pure, low-surface-area manganese oxide reference compounds are shown in Fig. 4. MnO_2 is Raman inactive (trace a) and Mn_2O_3 shows very weak bands at 697, 653, and 311 cm^{-1} (trace b). MnO is Raman active, with bands around 1030, 648, 544, and 306 cm^{-1}. Mn_3O_4 exhibits the strongest Raman bands, with a strong band at 654 cm^{-1} and smaller bands at 368 and 316 cm^{-1}. The corresponding high-surface-area manganese oxide samples, MnO_2 prepared from calcination of manganese nitrate or carbonate

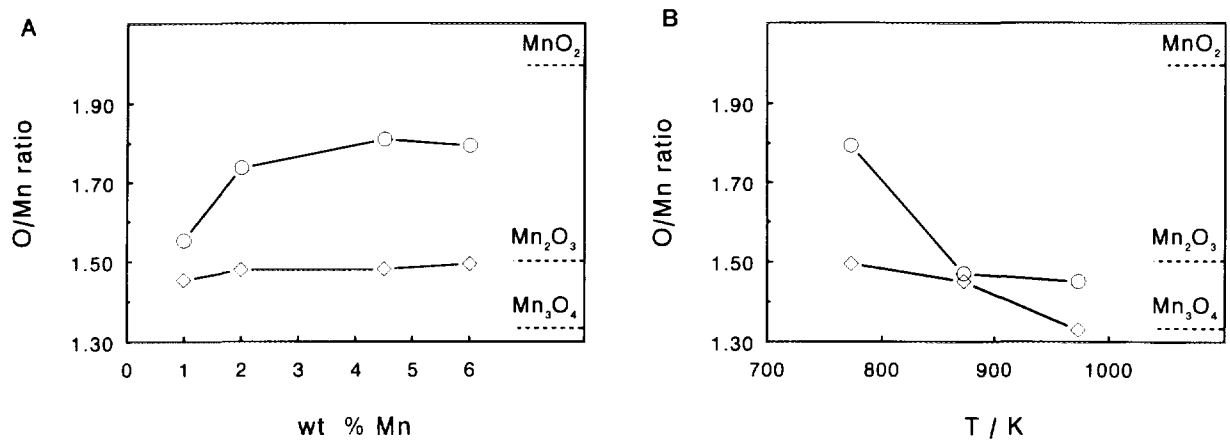

FIG. 2. Average stoichiometric O/Mn ratio in the catalyst samples, (A) as a function of the Mn loading and (B) as a function of temperature for 6 wt% Mn: ◇, ex-acetate; ○, ex-nitrate.

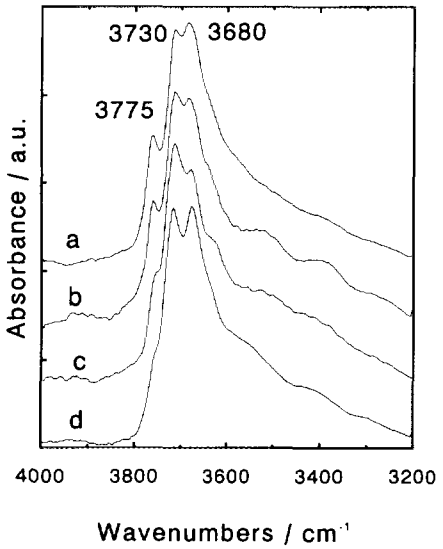

FIG. 3. IR spectra of the hydroxyl stretching region under dehydrated conditions (air, 770 K). (a) γ-Al_2O_3; (b) 2 wt% and (c) 6 wt% Mn (ex-acetate)/γ-Al_2O_3; (d) 2 wt% Mn (ex-nitrate)/γ-Al_2O_3.

in oxygen at 670 K and Mn_2O_3 prepared from manganese acetate or carbonate by calcination in oxygen at 825 K (14, 27), also exhibit the spectrum of the Mn_3O_4, but the signals are somewhat weaker. The average stoichiometry and structure of these samples have been confirmed by TPR and XRD (14, 27). The manganese aluminate sample exhibited weak bands at 204, 396, 416, 512, 643, and 776 cm^{-1}.

The Raman spectra of the alumina-supported Mn oxide

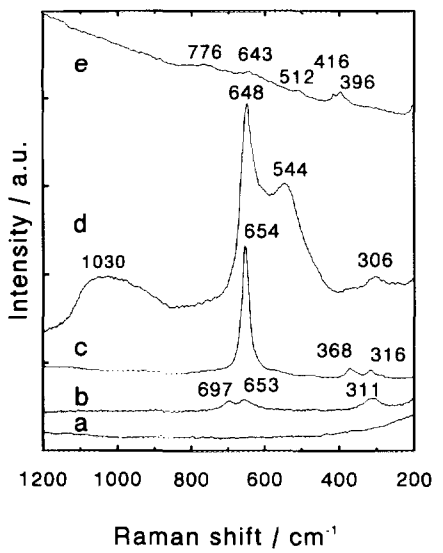

FIG. 4. Raman spectra of (a) MnO_2, (b) Mn_2O_3, (c) Mn_3O_4, (d) MnO, and (e) $MnAl_2O_4$ under ambient conditions.

catalyst samples are presented in Figs. 5. All ex-acetate samples, except for the 8.4 wt% Mn, exhibit a broad Raman band that centers around 637 cm^{-1}. Other minor features are also observed, especially a weaker shoulder at 730–765 cm^{-1}. The Raman spectra of the ex-nitrate samples (Fig. 5B) reveal qualitatively the same behavior; however, they differ in the position of the main Raman band which is at 650–653 cm^{-1} for all the samples, with the exception of the 1 wt% Mn sample (trace a) which possesses a band at 643 cm^{-1}. The second difference between the two preparations is the width of the major Raman band, which is much broader for the ex-acetate samples than for the ex-nitrate samples.

X-Ray Photoelectron Spectroscopy

The Mn $2p_{3/2}$ and $2p_{1/2}$ photoelectron binding energies of the reference Mn oxide compounds, corrected for charging by reference to the C 1*s* peak, are presented in Table 2. In general these values agree with the literature (22, 31–33), although much scatter can be noted in the values for the manganese oxides. There is a trend toward decreasing binding energy with decreasing oxidation state. Some representative XPS spectra of the Mn 2*p* region are given in Fig. 6. The binding energies of the Mn $2p_{3/2}$ electrons of the catalysts are plotted as a function of Mn loading in Fig. 7. The 1 wt% Mn/alumina samples have the highest binding energy (B.E.) values, higher than those of the reference Mn oxide compounds. With increasing loading the values for ex-acetate samples decrease somewhat, but remain relatively high. For the ex-nitrate samples, binding energy drops to a constant value for samples containing more than 1 wt% Mn.

The XPS signal intensity ratio Mn $2p_{3/2}$/Al 2*p* of the uncrushed catalyst particles increases fairly linearly as a function of loading (Fig. 8) for both preparations, the ratio of the ex-nitrate samples being higher than that of the ex-acetate samples. After the samples are powdered, the results for the ex-acetate samples remained unaltered, whereas the signal intensity ratio for the ex-nitrate samples had decreased considerably.

DISCUSSION

The studies characterizing the alumina-supported manganese oxide catalysts clearly demonstrate that the manganese oxide phases prepared from acetate and nitrate precursors are very different. Catalysts prepared from the nitrate precursor exhibit many properties characteristic of bulk manganese oxide compounds and suggest that the manganese oxide component is present as microcrystalline particles on the alumina support. The manganese oxide XPS binding energies are fairly similar to those for bulk manganese oxide reference compounds. TPR measurements give rise to sharp reduction peaks that do not

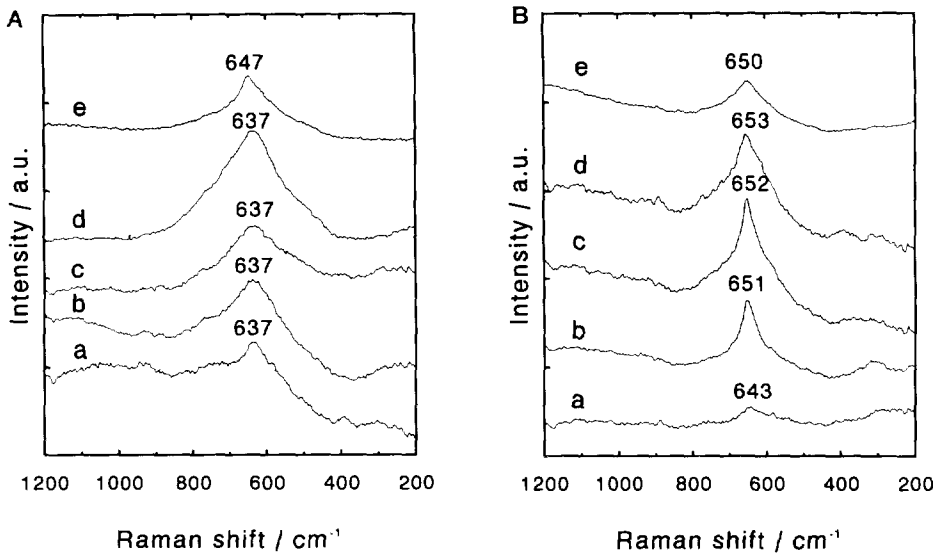

FIG. 5. Raman spectra of manganese oxide/alumina samples for different Mn loadings, under ambient conditions: (A) ex-acetate, (B) ex-nitrate. Mn loading: (a) 1 wt%, (b) 2 wt%, (c) 4.5 wt%, (d) 6 wt%, (e) 8.4 wt%.

TABLE 2

Observed Binding Energy (eV) of the Mn 2*p* Photoelectrons in Mn Reference Compounds

Sample	This study		Literature[a]
	Mn $2p_{1/2}$	Mn $2p_{3/2}$	Mn $2p_{3/2}$
MnO_2	653.2	641.6	641.1–642.4
Mn_2O_3	653.0	641.3	641.2–641.9
Mn_3O_4	653.1	641.4	641.3–641.4
MnO	653.1	641.4	640.6–641.7
$MnAl_2O_4$	653.8	641.8	641.6

[a] References (22, 31–33).

shift appreciably with Mn loading and are characteristic of bulk manganese oxide compounds (especially the reduction via two stages) (27). The Raman bands are relatively narrow, similar to those of bulk manganese oxide phases. XRD could not detect these microcrystalline (4 nm or below) manganese oxide phases because they are apparently below the detectability of XRD, in agreement with the evaluation of the XPS data in Fig. 8.

In contrast, catalysts prepared from the acetate precursor exhibit many properties characteristic of a highly dispersed surface manganese oxide phase on alumina. The Mn $2p_{3/2}$ electron binding energy is higher than that observed for the pure bulk manganese oxides and reflects the interaction of Mn with the alumina environment. Similar

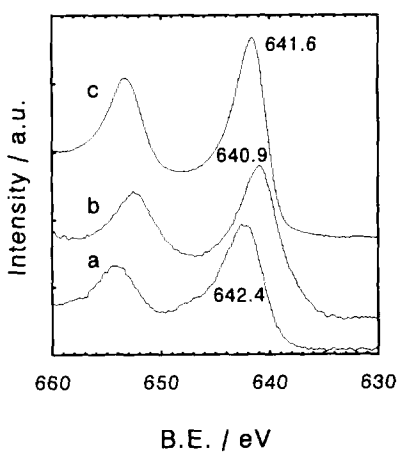

FIG. 6. XPS spectra of the Mn 2*p* region: (a) 4.5 wt% Mn (ex-acetate); (b) 4.5 wt% Mn (ex-nitrate); (c) MnO_2.

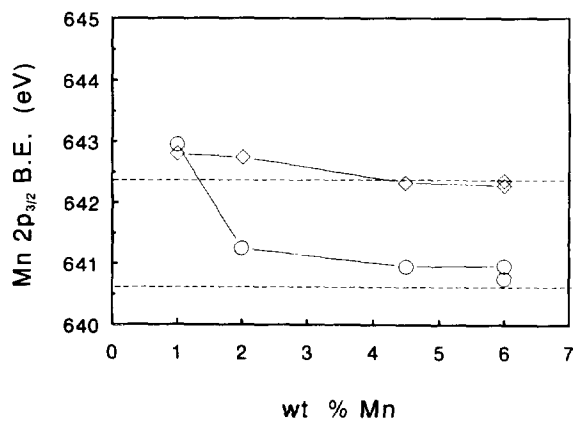

FIG. 7. Mn $2p_{3/2}$ photoelectron binding energy as a function of Mn loading. Dashed lines indicate the region of values for pure Mn oxides (Table 2). ◇, Ex-acetate; ○, ex-nitrate.

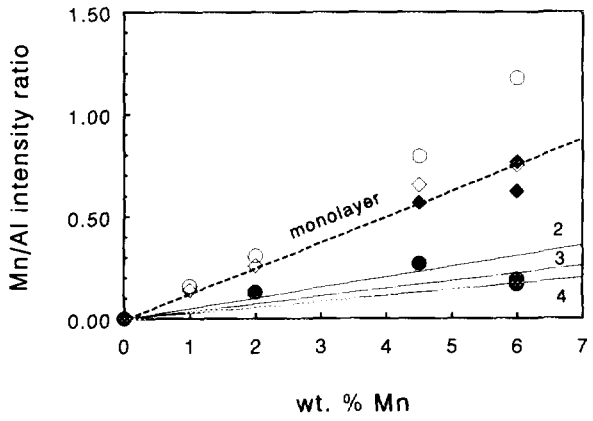

FIG. 8. XPS Mn $2p_{3/2}$/Al $2p$ intensity ratio as a function of Mn loading. ◇, ◆: ex-acetate; ○, ●: ex-nitrate. Open symbols: particles, closed symbols: crushed samples. Included are relations for monolayer catalyst (dashed line) and catalysts with microcrystals of 2, 3, and 4 nm (solid lines).

shifts in binding energy have previously been reported for other two-dimensional surface metal oxide phases on alumina (34–37). Manganese oxide reduction during TPR gives rise to broad peaks which shift with coverage as found for other alumina-supported surface metal oxide systems, e.g., (35, 36). The supported manganese oxide gives rise to broad Raman bands which are shifted relative to the corresponding bulk metal oxides (38, 39). Thus, the Mn oxide in the alumina-supported catalyst formed from the nitrate precursor is mainly present as a microcrystalline material, whereas that formed from the acetate precursor is primarily present as a surface metal oxide.

The characterization data suggest that the supported manganese oxide catalysts do not contain a single manganese oxide phase, but are a mixture of oxides. The TPR experiments for the ex-nitrate samples reveal an O/Mn stoichiometry of 1.8, which is between those of MnO_2 and Mn_2O_3, but the Raman spectra, which are especially sensitive to the Mn_3O_4 phase, also reveal the presence of this compound. Thus, it appears that all three oxides are present in the samples from the nitrate precursor. In addition, the 1 wt% Mn/alumina (ex-nitrate) sample possesses TPR, XPS, and Raman features characteristic of a surface manganese oxide, as for the ex-acetate samples. The TPR experiments on ex-acetate catalysts reveal an O/Mn ratio of 1.5 which would correspond to Mn_2O_3, but the exact stoichiometry of this surface manganese oxide phase is not clear since it shares oxygen atoms with the alumina via Mn–O–Al bonds.

Infrared Spectroscopy

The IR spectra of the hydroxyl region for the alumina-supported metal oxide phases usually provides information about the interaction of the metal oxide phases with the support. Surface metal oxide phases containing high-valent metal oxides appear to coordinate preferentially to the surface hydroxyls of the alumina, whereas low-valent metal oxides appear to coordinate preferentially to alumina coordinatively unsaturated sites (39). The IR results suggest that the preparation route can influence this trend; this is explained by an ion pairing process with the alumina surface as follows (40). In the acidic manganese nitrate solution the following equilibria exist between the solvated manganese ion complexes:

$$\underset{\textbf{(A)}}{Mn^{2+}(OH_2)_4} \rightleftarrows \underset{\textbf{(B)}}{Mn^{2+}(OH^-)(OH_2)_3} + H^+ \rightleftarrows \underset{\textbf{(C)}}{Mn^{2+}(OH^-)_2(OH_2)_2} + 2H^+ \quad (1)$$

In this solution, especially the basic hydroxyl groups of the alumina surface will be protonated. Subsequently, an ion pairing process can take place between these protonated hydroxyls and the manganese complexes **B** and **C**, leading to type I surface complex (see Scheme 1). This

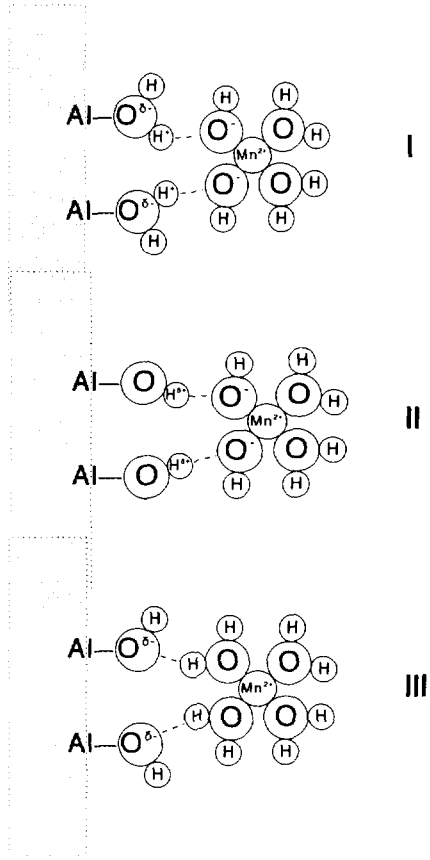

SCHEME 1

accounts for the observation of a decrease in the stretch vibration of the most basic groups at 2 wt% Mn loading. In the case of an acetate solution the pH is higher (6.7–7.5) due to the acetic acid equilibrium, which takes away protons and shifts Eq. (1) to the right. The pH is about equal to that of the zero protonation charge (ZPC) value of the alumina. Therefore, the alumina surface will be unaltered, and by electrostatic interaction the acidic hydroxyl groups will form a complex with the (negative) oxygen anion side of manganese complexes **B** and **C** (type II). Consequently for the ex-acetate samples a pronounced decrease in the 3680 cm^{-1} band is observed in FTIR spectra, indicating that the acetate preparation route selectively deposits Mn ions at the acidic –OH groups up to 2 wt%. At higher loadings the acidic surface hydroxyls become exhausted and the solvated Mn ion **A** starts to interact with the (slightly negative) basic hydroxyl groups, yielding a complex of type III, accounting for the decrease in the OH stretch vibration at 3775 cm^{-1}.

Part of these processes can occur during the drying step since anionic groups of the manganese salts are partially being removed as NO/NO_2 or as HAc gas. Finally, solvating water is removed and condensation occurs, resulting in Al–O–Mn bond formation.

On calcination the Mn(II) is oxidized to Mn(III). Although this ion–support interaction is depicted for the aqueous phase, the interaction of the Mn ion with the alumina surface is probably so strong that it survives the calcination procedure and results in a highly dispersed manganese oxide surface phase.

It is noted that the estimated number of surface hydroxyl groups on γ-alumina amounts to about 10 per square nanometer, distributed in a 2:6:2 ratio over the acidic, neutral, and basic groups (29). Assuming that the hydroxyl groups are the anchoring sites for manganese ions in a 2/1 OH/Mn^{2+} ratio, a monolayer coverage would be reached at about 8 wt% Mn loading (see Table 1). Hence, a loading of 2 wt% Mn would be sufficient to cover all acidic or basic OH groups and can account for the decrease in the intensity of the IR absorption bands of the most acidic and basic OH groups at 6 wt% loading for the ex-acetate sample. This is confirmed by the work of Wakker *et al.* (20) who could easily deposit 8 wt% Mn by ion exchange with a manganese acetate solution.

Probably not all the manganese ions are deposited in this way, especially at the highest loadings. The rest are deposited as the precursor complex $MnAc_2 \cdot 4H_2O$. The distance between the manganese cations in this complex is relatively large and impedes the possible agglomeration during calcination, which can also contribute to the good dispersion.

By contrast the nitrate samples indicate that only initially an exchange with basic hydroxyls occurs (type I, below 2 wt% Mn), which is followed by further deposition of the nitrate on drying. The deposited nitrate is known to decompose already at low temperatures, between 370 and 500 K (23), and apparently the nitrogen dioxide and nitric oxide are able to oxidize the Mn(II) to Mn(IV) during this process. At higher loadings clusters or small crystallites of oxide are to be expected since nitrates usually are deposited in crystalline form, due to the absence of a strong interaction with the alumina surface.

The present multistep impregnation procedure apparently yields better dispersions than a one-step impregnation (25, 41). XRD did not reveal crystalline material up to 8.4 wt% Mn, whereas others observed XRD patterns at loadings above 2.5 wt% Mn (21, 22). The partial decomposition of the nitrate during the drying step may have contributed to the higher dispersion, since redissolution of the nitrate in the consecutive impregnation step, with the potential formation of larger clusters, is prevented.

Temperature-Programmed Reduction

The average stoichiometry of the manganese oxide on the ex-acetate samples corresponds to that of Mn_2O_3, with the exception of the 1 wt% Mn loading sample, which is slightly lower. The ex-nitrate samples exhibit a stoichiometry between those of Mn_2O_3 and MnO_2, and approach the latter with increasing Mn loading. Above 1 wt% Mn the TPR patterns of the ex-nitrate samples resemble those of the reduction of the pure Mn oxides. Mn_2O_3 and MnO_2 both reduce first in one step to Mn_3O_4 and in a second step to MnO (27). Although XRD did not reveal crystalline material, small oxidic clusters should be present on the ex-nitrate samples to exhibit a reduction behavior like that of the pure oxides. This is supported by the XPS data (see below) and by the absence of a clear shift in reduction temperature as a function of loading, which indicates the absence of a strong interaction with the alumina.

Calcination at 870 and 970 K results in the formation of the thermodynamically more stable Mn_2O_3 phase, in agreement with the XRD results of Strohmeier and Hercules (22). The observed hydrogen consumption ratio of 1:2 for the first and second reduction steps is in excellent agreement with the intermediate Mn_3O_4 formation. The TPR results for the ex-nitrate samples support the conclusions in the literature (21–26), based on other techniques, with regard to stoichiometry of the oxide and cluster formation.

The broad convolution of reduction peaks for the ex-acetate samples (Fig. 1A) indicates a much stronger interaction of a quite heterogeneous nature, suggesting a highly dispersed system. This interaction decreases with increasing Mn loading since the major reduction profile shifts to lower temperatures. At around 840 K a constant amount of manganese oxide is reduced, relative to the amount of

alumina, viz., about 0.3 wt% Mn, corresponding to 36 μmol Mn(III)/g alumina or 0.11 atoms of Mn(III)/nm^2. Also, Lo Jacono and Schiavello (8) observed a constant amount of Mn^{2+} on their catalysts of the same order of magnitude (0.2–0.5 wt%). This amount could not be oxidized, so a relation with our surface species seems not to be present. The Mn(III) species that reduces at around 840 K must interact strongly with the alumina surface, to explain why the reduction takes place at higher temperatures. This reduction will be a one-step reduction of Mn(III) to Mn(II), since due to the high dispersion no stable intermediate Mn_3O_4 phase can be formed. This one-step reduction is also observed for alumina-supported tungsten oxide (35, 38).

The major reduction process between 500 and 700 K for 1 and 2 wt% Mn loading (Fig. 1A, traces b and c) also points to a one-step reduction process. In a two-step reduction a hydrogen consumption ratio of 1 : 2 for the two steps is expected, which cannot be deduced from the reduction pattern. Although a small reduction can be perceived for the 2 wt% Mn sample at around 500 K, the amount is too small. Again, a one-step reduction of Mn(III) to Mn(II) points to high dispersion, since then a stable intermediate Mn_3O_4 phase cannot be formed. This Mn_2O_3 is envisaged as an epitaxial layer on the alumina support, with which it is isomorphous. The Mn(III) is probably present at the surface in octahedral symmetry, since only Mn(II) prefers a tetrahedral site (24). Above 2 wt% Mn the reduction in the temperature region around 480–500 K increases considerably, relative to that around 600 K, and shifts to lower temperatures with increasing loading, indicating a decreasing interaction with the alumina (Fig. 1A, traces d–f). These facts suggest that one or more adlayers of Mn_2O_3 have been formed which allow a two-step reduction via Mn_3O_4. It is noted that the dispersion must still be high since the reduction takes place at considerably lower temperatures than for the ex-nitrate samples (Fig. 1B).

The heat treatment of the 6 wt% sample supports this formation of adlayers of Mn_2O_3, since the amount reduced around 480–500 K has decreased, resulting in an average stoichiometry of Mn_3O_4.

X-Ray Photoelectron Spectroscopy

XPS results indicate that the ex-acetate samples exhibit a systematic shift in the Mn $2p_{3/2}$ binding energy position, from 642.8 to 642.3 eV, with increasing Mn loading. This value is quite high, about 1–1.5 eV higher, compared with those of the pure oxides, which are generally between 641 and 642 eV (22, 31–33). The location of the highly dispersed Mn(III) ions on the alumina surface results in a stronger electrostatic field for these ions in pure Mn_2O_3, due to the smaller ion radius of Al(III) (51 pm) compared with Mn(III) (66 pm) (42). The overall effect is a shift to higher binding energies. With increasing loading and the formation of adlayers of Mn_2O_3 this interaction diminishes and the average binding energy shifts to lower values. This higher binding energy has also been observed for La–alumina catalysts (37), for which an increase of up to 1.8 eV was observed. This was confirmed for a lanthanum β-aluminate ($La_2O_3 \cdot 11Al_2O_3$ (43) and supports the idea that this points to a highly dispersed system.

An interaction with the alumina is also noted for the 1 wt% Mn ex-nitrate sample, after which an abrupt decrease in binding energy occurs at higher loadings and which falls on the low side of the range of values reported in literature. The scatter in the literature data arises mainly from temperature treatment effects. Oku and Hirokawa (32) revealed that this resulted in a decrease in binding energy. This clearly applies also to the calcined ex-nitrate catalyst samples. Catalysts prepared by impregnation with ammonium permanganate solutions (4) also exhibited B.E. values between 641 and 642 eV, indicating a low interaction with the alumina.

A linear Mn $2p_{3/2}$/Al $2p$ intensity ratio is found as a function of Mn loading for the uncrushed particles of the ex-acetate samples, whereas a more than linear increase can be perceived for the ex-nitrate samples. In the latter case the values even exceed those of the monolayer catalyst, predicted by the method of Kerkhof and Moulijn (44) and based on the experimentally determined sensitivity for Al and Mn in $MnAl_2O_4$. This is typical of enrichment at the particle surface.

For the powdered ex-acetate samples the trend remained unchanged and exactly matched the predicted monolayer trend. The powdered ex-nitrate samples decreased considerably in Mn intensity which indicates that manganese oxide was present as small crystallites in the outer shell of the original alumina particles. In Fig. 7 the predicted intensity ratio trends are included for 2-, 3-, and 4-nm particles. These indicate that for the ex-nitrate catalysts the microcrystallite size is between 2 and 4 nm, and below the XRD detection limit. This result also demonstrates the applicability of XPS in determining particle sizes of supported catalysts (44, 45).

Enrichment at the outer regions of catalyst particles after impregnation with nitrate precursors has been reported at various times and is discussed extensively by van der Brink (46). This enrichment is generally attributed to the rate of drying and to capillary forces in the micropores of the support particles. Another explanation, however, is based on a study similar to the present one but for alumina-supported Co oxide, also prepared from nitrate and from acetate (34). These authors noted by XPS that the distribution of Co was fairly uniform throughout the particles after the impregnation and drying step in the nitrate preparation route. Only after the calcination step

was the enrichment at the outer shell of the particles observed. Thus, agglomeration takes place during the calcination step. Probably this also applies to the ex-nitrate Mn catalyst samples.

Raman Spectroscopy

The Raman spectra of the alumina-supported Mn oxide samples are of a high quality. Only Strohmeier and Hercules (22) previously applied this characterization technique to Mn oxide catalysts, but could not measure any signal intensity. Only Mn_3O_4 and, to a lesser extent, MnO are Raman active. Therefore, only the Raman band of Mn_3O_4 is observed at about 652 cm^{-1} for the ex-nitrate samples. This corresponds nearly exactly with the band position of bulk Mn_3O_4 (654 cm^{-1}), which represents a single Mn–O bond vibration. The high-surface-area MnO_2 and Mn_2O_3 samples also exhibited Raman bands at 654 cm^{-1}, indicating that these materials were not phase pure even though their oxidation state is 4+ and 3+. The high Raman sensitivity for Mn_3O_4 overemphasizes the presence of this phase in the catalyst compared with MnO_2 and Mn_2O_3. The ex-acetate samples exhibit broad Raman bands shifted to lower wavenumbers (around 637 cm^{-1}). This shift can also be seen for the 1 wt% ex-nitrate sample. Furthermore, the Raman bands are much broader for the ex-acetate samples than for the ex-nitrate samples which is characteristic of a surface metal oxide phase, in agreement with the TPR results.

Although XRD confirmed the successful preparation of $MnAl_2O_4$, its Raman spectrum shows only weak bands and does not correspond to that of Strohmeier and Hercules (22) who report strong bands at 472 and 393 cm^{-1}. They applied a longer reduction period (36 h) to obtain their sample, which may have led to a better developed structure. Pott and McNicol (24) showed by phosphorescence spectroscopy that Mn(II) has an exclusive preference for tetrahedral coordination and tends to fill lattice defects in the γ-Al_2O_3 surface, resulting in a basically tetrahedral-like symmetry. Higher-valent Mn will occupy octahedral sites. It was noted that after a calcination procedure our $MnAl_2O_4$ sample exhibited the Mn_3O_4 Raman spectrum, indicating instability of part of the structure. This is not surprising, since in a spinel structure the Mn(II) should occupy the tetrahedral holes, while its size is much larger than that of the hole in an ideally packed lattice, 80 pm versus 28 pm in radius (24). No clear indications are found from the Raman spectra for the formation of a surface $MnAl_2O_4$ phase as proposed by Lo Jacono and Shiavello (8), although some weak similarities should be noted in the region 600–800 cm^{-1} between the catalysts and the $MnAl_2O_4$ sample.

Evaluating the results as a whole, it is clear that the use of manganese acetate yields highly dispersed manganese oxide catalysts due to two effects. First, there is the electrostatic interaction between manganese cations and the acidic and basic surface hydroxyl groups at the alumina surface, aided by the weak acidic character of the acetic acid, and second, the absence of the tendency of the manganese complex to agglomerate at higher loadings and during calcination, as happens with the nitrate. Baltanas *et al.* (26) proposed the preparation by precipitation of $Mn(OH)_2$ during the drying step by treatment with ammonia. XRD confirmed the higher dispersion but this preparation seems more laborious than the incipient wetness method using the acetate salt. Moreover, no additional data, such as the IR results of this study, are available for their catalysts that indicate a preferential deposition at certain surface sites. Recently, van der Kleut (16) applied a manganese–EDTA complex to prepare an alumina-supported manganese oxide catalyst, with similar TPR results as in this study.

This comparative study of two different precursors confirms that temperature-programmed reduction is a powerful technique to characterize oxidic catalysts. The reduction profile can give a clear indication about the dispersion and interaction with the support surface, although it will provide only an average stoichiometry of the oxidic phase and will not yield a discrimination between species in different oxidation states, in contrast to certain physicochemical techniques. The XPS results demonstrate the usefulness of this technique to determine dispersion, distribution, and particle sizes of supported active phases and the interaction of the active phase with the support.

The catalysts characterized here are very active in the low-temperature (350–500 K) selective catalytic reduction of NO with NH_3 and will be the subject of following papers on the mechanism and kinetics of this reaction. In view of the wide range of applications (1–19), it would be worthwhile to explore further the properties of the ex-acetate samples.

CONCLUSIONS

The preparation of alumina-supported manganese oxide catalysts by using manganese acetate as precursor results in a highly dispersed oxidic phase with Mn_2O_3 as average stoichiometry. This is due to the ionic interactions with acidic (up to 2 wt% Mn) and basic (above 2 wt% Mn) surface –OH groups of the alumina. Up to about 2 wt% Mn loading a monolayer structure is formed, whereas at higher loadings probably also multilayers are present. Hence, at low loadings a one-step reduction is observed, Mn(III) → Mn(II), whereas at higher loadings the reduction proceeds partially via the intermediate formation of a Mn_3O_4 phase.

Manganese nitrate yields only below 1 wt% Mn a dispersion comparable to that of the acetate precursor. At higher

loadings microcrystals of manganese oxide, 2–4 nm in size and with an average oxidation state between 3+ and 4+, are obtained on the surface, and these behave like pure oxides. Multiple-step impregnation, however, does yield better dispersions than one-step preparations reported in the literature for ex-nitrate catalysts. These manganese oxide microcrystals exhibit the two-step reduction behavior of the pure oxides MnO_2 and Mn_2O_3.

Temperature-programmed reduction is an excellent characterization technique for oxidic supported catalysts, especially because amorphous systems can be studied well. XPS is quite useful to determine distributions of active phases in particles and the size of microcrystals below the XRD limit of common instruments.

REFERENCES

1. Döbereiner, J. W., *Schweigger's J. Chem. Phys.* **28,** 247 (1820).
2. Kanungo, S. B., *J. Catal.* **58,** 419 (1979).
3. Mooi, J., and Selwood, P. W., *J. Am. Chem. Soc.* **74,** 1750 (1952).
4. Nohman, A. K. H., Duprez, D., Kappenstein, C., Mansour, S. A. A., and Zaki, M. I., *in* "Preparation of Catalysts V" (G. Poncelet, P. A. Jacobs, P. Grange, and B. Delmon, Eds.), p. 617. Elsevier, Amsterdam, 1991.
5. Katz, K., *Adv. Catal.* **5,** 177 (1953).
6. Boreskov, G. K., *Adv. Catal.* **15,** 285 (1964).
7. Innes, W. B., *in* "Catalysis" (P. H. Emmett, Ed.), Vol. 2, Ch. 1. Reinhold, New York, 1955.
8. Lo Jacono, M., and Schiavello, M., *in* "Preparation of Catalysts" (B. Delmon, P. A. Jacobs, and G. Poncelet, Eds.), p. 474. Elsevier, Amsterdam, 1976.
9. Nishino, A., *Catal. Today* **10,** 107 (1991).
10. Baltanas, M. A., Stiles, A. B., and Katzer, J. R., *Appl. Catal.* **28,** 13 (1986).
11. Dmuchovsky, B., Freeks, M. C., and Zienty, F. B., *J. Catal.* **4,** 577 (1965).
12. Il'Chenko, N. I., and Golodets, G. I., *J. Catal.* **39,** 57 (1975).
13. Singoredjo, L. S., Korver, R. B., Kapteijn, F., and Moulijn, J. A., *Appl. Catal. B Environ.* **1,** 297 (1992).
14. Singoredjo, L., "Low Temperature Selective Catalytic Reduction of Nitric Oxide with Ammonia." Ph.D. thesis, University of Amsterdam, 1992.
15. Karlsson, H. T., and Rosenberg, H. S., *Ind. Eng. Chem. Process Des. Dev.* **23,** 808 (1984).
16. Van der Kleut, D., Ph.D. thesis, University of Utrecht, The Netherlands, 1994.
17. Burch, R., Chalker, S., Squire, G. D., Shik Chi Tsang, *J. Chem. Soc. Faraday Trans.* **86,** 1607 (1990).
18. Moggridge, G. D., Rayment, T., and Lambert, R. M., *J. Catal.* **134,** 242 (1992).
19. Markvart, M., and Pour, V., *Int. Chem. Eng.* **15,** 546 (1975).
20. Wakker, J. P., Gerritsen, A. W., and Moulijn, J. A., *Ind. Eng. Chem. Res.*, **32,** 139 (1993).
21. Cavallaro, S., Bertuccio, N., Antonucci, P., Giordano, N., and Bart, J. C., *J. Catal.* **73,** 337 (1982).
22. Strohmeier, B. R., and Hercules, D. M., *J. Phys. Chem.* **88,** 4922 (1984).
23. Selwood, P. W., Moore, T. E., and Ellis, M., *J. Am. Chem. Soc.* **71,** 693 (1949).
24. Pott, G. T., and McNicol, B. D., *Discuss. Faraday Soc.* **52,** 121 (1971).
25. Burlamacchi, L., and Villa, P. L., *React. Kinet. Catal. Lett.* **3,** 199 (1975).
26. Baltanas, M. A., Stiles, A. B., and Katzer, J. R., *J. Catal.* **88,** 362 (1984).
27. Kapteijn, F., Singoredjo, L., Andreini, A., and Moulijn, J. A., *Appl. Catal. B Environ.* **3,** 173 (1994).
28. Monti, D. A., and Baiker, A., *J. Catal.* **83,** 323 (1983).
29. Knözinger, H., and Ratnasamy, P., *Catal. Rev. Sci. Eng.* **17,** 31 (1978).
30. Van Veen, J. A. R., Jonkers, G., and Hesselink, W. H., *J. Chem. Soc. Faraday Trans. I* **85,** 389 (1989).
31. Wöllner, A., Lange, F., Schmelz, H., and Knözinger, H., *Appl. Catal. A Gen.* **94,** 181 (1993).
32. Oku, M., and Hirokawa, K., *J. Electron. Spectrosc. Relat. Phenom.* **7,** 465 (1975).
33. Brabers, V. A. M., Van Setten, F. M., and Knapen, P. S. A., *J. Solid. State Chem.* **49,** 93 (1983).
34. Okamoto, Y., Adachi, T., Nagata, K., Odawara, M., and Imanaka, T., *Appl. Catal.* **73,** 249 (1991).
35. Thomas, R., de Beer, V. H. J., and Moulijn, J. A., *Bull. Soc. Chim. Belg.* **90,** 1349 (1981).
36. Arnoldy, P., Bruinsma, O. S. L., and Moulijn, J. A., *J. Mol. Catal.* **30,** 11 (1985).
37. Haack, L. P., de Vries, J. E., Otto, K., and Chatta, M. S., *Appl. Catal. A Gen.* **82,** 199 (1992).
38. Wachs, I. E., Chersich, C. C., and Hardenbergh, J. H., *Appl. Catal.* **13,** 335 (1985).
39. Turek, A. M., Wachs, I. E., and DeCanio, E., *J. Phys. Chem.* **96,** 5008 (1992).
40. Che, M., *in* "Proceedings, 10th International Congress on Catalysis, Budapest, 1992" (L. Guczi, F. Solymosi, and P. Tétényi, Eds.), p. 31. Akadémiai Kiadó, Budapest, 1993.
41. Wakao, N., Smith, J.M., and Selwood, P. W., *J. Catal.* **1,** 62 (1962).
42. Weast, R. C. (Ed.), "Handbook of Chemistry and Physics," Vol. 67, p. F157. CRC Press, Boca Raton, FL, 1987.
43. Haack, L. P., Peters, C. R., de Vries, J. E., and Otto, K., *Appl. Catal. A Gen.* **87,** 103 (1992).
44. Kerkhof, F. P. J. M., and Moulijn, J. A., *J. Phys. Chem.* **83,** 1612 (1979).
45. Kaliaguine, S., Adnot, A., and Lemay, G., *J. Phys. Chem.* **91,** 2886 (1987).
46. Van der Brink, P. J., "The Selective Oxidation of Hydrogen Sulphide to Elemental Sulphur on Supported Iron-Based Catalysts." Ph.D. thesis, University of Utrecht, 1992.